Christian Ergenzinger
Research Associate
e-mail: christian.ergenzinger@itm.uni-stuttgart.de

Robert Seifried
Junior Professor
e-mail: robert.seifried@itm.uni-stuttgart.de

Peter Eberhard[1]
Professor and Director
e-mail: peter.eberhard@itm.uni-stuttgart.de

Institute of Engineering
and Computational Mechanics,
University of Stuttgart,
70569 Stuttgart,
Germany

A Discrete Element Approach to Model Breakable Railway Ballast

A discrete element approach to assess degradation processes in ballast beds is presented. Firstly, a discrete element model describing strength and failure of strong rock is introduced. For this purpose a granular solid is created by bonding of adjacent particles. A method to define angular ballast stones made from the granular solid is proposed. The strength of these stones is evaluated by compression between parallel platens. Comparing these results to published experimental data yields very good qualitative and reasonable quantitative agreement. Finally, the failure of aggregates of breakable stones is investigated by simulation of oedometric compression tests and indentation of a sleeper into a ballast bed. [DOI: 10.1115/1.4006731]

1 Introduction

Ballast degradation and track settlement have become increasingly important problems due to higher train speeds and axle loads. Methods that increase lateral stresses in tracks have been proposed to reduce settlement and ballast degradation. Such methods are, e.g., the insertion of geogrids [1] or the use of winged sleepers or lateral restraints between the sleepers [2]. However, it is expensive and time consuming to conduct experiments that are necessary to develop an in-depth understanding of the phenomena occurring inside of the ballast and that help in designing improved reinforcement devices. By numerical simulation the behavior of the ballast can be assessed up to some level of detail, if an adequate model is provided. While finite element or multibody models allow for simulation of the track with respect to vehicle dynamics (see, e.g., Refs. [3–6]), models that account for the discrete nature of the ballast are required to compute phenomena occurring inside of the track bed.

The discrete element method (DEM) [7] has previously been applied to investigate the behavior of railway ballast [8–10]. Published simulation approaches are often based on geometrically simple shapes, i.e., disks or spheres, of the breakable bodies [8,9]. Different approaches to create complex shaped stones have been proposed [11,12], but they are not able to consider breaking or degradation processes. In this contribution, a discrete element model is presented, which models ballast as a set of angular stones that themselves are made of breakable rock material. Thus, the presented model unites both aforementioned aspects by consideration of breakable bodies of complex shape. Ballast fouling by breakage and abrasion of the stones is inherently present in the model.

The paper is organized as follows. Firstly, a discrete element model is described, which captures strength and failure properties of strong rock by creation of a granular solid consisting of bonded spherical particles. Then, an approach to generate angular ballast stones made from this granular solid is proposed. The strength of these stones is investigated by compression between parallel platens and compared to experimental results from literature. Finally, aggregates of breakable stones are constructed and the degradation processes in typical load cases are simulated.

2 Discrete Element Modeling of Strong Rock

The DEM can be easily extended to the simulation of granular solids by introducing lasting particle bonds that generate forces even in case of negative overlap, i.e., a gap, between two bonded particles. A variety of particle bonding concepts was developed in the last 10 to 15 years and applied to different problems mainly in geomechanics and physics; see, e.g., Refs. [13–19]. Modeling of rock material by using breakably bonded spherical particles is usually considered the most viable approach [8,13,15,18–23] and also pursued in this research.

A granular solid is generally created by bonding adjacent particles from a dense packing. Fracture and failure phenomena can be easily incorporated in these models by removal or weakening of bonds based on suitable failure criteria. The advantage of this approach is that multiple fractures at arbitrary locations of the solid may happen. It is not necessary to initiate cracks as it is often the case in extended finite element methods [24]. The crack path is only limited by the discretization, i.e., fracture occurs on the level of bonds between unbreakable particles. For sufficiently small particles this states no serious limitation. Bond breakage based on the loading condition and system dynamics causes cracks to propagate, bifurcate, or coalesce. The simulations are performed on a meso-scale in order to capture the global behavior of the breakable ballast, while the micromechanical details of crack propagation are not of interest.

2.1 Dense Sphere Packings.

The generation of a suitable initial configuration is the first step of every DEM simulation. In case of simulations dealing with bonded particles this initial configuration is a dense packing of particles that is then bonded. A variety of approaches exists for the generation of such a packing; see, e.g., Ref. [25] and references therein. A homogeneous and isotropic sphere packing can be obtained by compression of the volume containing the particles or by expansion of the particles inside of a fixed domain.

It is proposed in Ref. [26] to employ a radius expansion scheme that introduces a dependency of a particle's individual normalized growth rate $\dot{r}(t)/r(t)$ on its coordination number c_n. The scheme reads

$$\dot{r}(t)/r(t) = \max\left(\dot{R}[1 - c_n(t)/\hat{c}_n],\ 0\right) \tag{1}$$

where $\dot{R}$ is the maximal growth rate and $\hat{c}_n$ denotes a "desired" coordination number that serves as a further control parameter for the inflation procedure. It was shown in Ref. [27] that this scheme

[1]Corresponding author.

Contributed by Design Engineering Division of ASME for publication in the Journal of Computational and Nonlinear Dynamics. Manuscript received October 19, 2011; final manuscript received April 9, 2012; published online June 22, 2012. Assoc. Editor: Khaled E. Zaazaa.

leads to an increase of the average coordination number compared to standard procedures while particle overlap, i.e., stored deformation energy, is kept small.

2.2 Bonding Concept. Particle bonds usually correspond to force laws that act in restricting at least one degree of freedom of the relative motion of the bonded particles. In this study, the bonds are limited to the normal direction and are represented by springs that act between the centers of the bonded particles, i.e., a central force model is considered. Shear, bending, and twisting are not inhibited [16,28]. For a detailed description of this model see Ref. [27]. All simulations described in this paper are performed using the software package Pasimodo [29,30].

Bonds are created between particles that overlap in the very first time step at time $t = 0$. The contact force results from the bond as long as it is intact. For particles that are not or no longer bonded a repulsive interaction is applied. In both cases the contact or bond force is calculated as a linear function of overlap and relative normal velocity. Bond breakage is allowed in tension and compression with different strengths.

In contrast to real rock, bonded particle models do not feature singular stress concentrations near crack tips and instable crack propagation [15]. Therefore, a progressive failure model is introduced [27,31]. This failure model locally accumulates damage in such a way that the strength R_m of a bond between two particles i and j is calculated according to

$$R_m(t) = \hat{R}_m \left(\frac{n_{c,i}(t) n_{c,j}(t)}{n_{c,i,}(0) n_{c,j}(0)} \right)^a \tag{2}$$

where $\hat{R}_m$ is the bond strength in undamaged material and $n_{c,\iota}$, $\iota = i, j$ is the number of a particle's bonds. The exponent a is chosen as the limited, weighted sum of the involved particles' number of broken bonds

$$a = \min\left(\alpha[n_{b,i}(t) + n_{b,j}(t)],\ b\right) \tag{3}$$

where α is a weighting factor, b denotes a maximal exponent, and the number of broken bonds is $n_{b,\iota}(t) = n_{c,\iota}(0) - n_{c,\iota}(t)$. Thus, breakage of the bonds of a particle will successively reduce the strength of the remaining bonds of this particle.

This concept inverts the idea of singular stress peaks, as it reduces the material strength near a point where a stress singularity should appear but cannot in simulation due to the particulate nature of the material. Nevertheless, the result is comparable, as in both cases the probability of further damage occurring near this point is increased.

In addition to the progressive failure model, unbreakable particle clusters are introduced in order to generate local heterogeneity, i.e., deformation incompatibilities, while keeping on the large scale homogeneity and isotropy [27]. Intracluster stiffness is chosen five times higher than between particles that do not belong to the same cluster or that are not part of any cluster. The higher intracluster stiffness assures that the deformation concentrates at the interfaces between clusters or in the nonclustered areas. Thus, the probability of failure is increased in these regions. An even higher intracluster stiffness is not necessary for this purpose and is avoided in order not to increase the particle eigenfrequencies requiring smaller time step sizes for numerical time integration.

2.3 Model Behavior. The strength of the granular solid created from bonding a dense ensemble of spheres is investigated in uniaxial and triaxial compression; see Refs. [27,32] for more details on the simulation setup and an in-depth analysis of the failure process. The model is calibrated and compared to granite as an example of a strong rock, which is widely used as ballast in railway track beds.

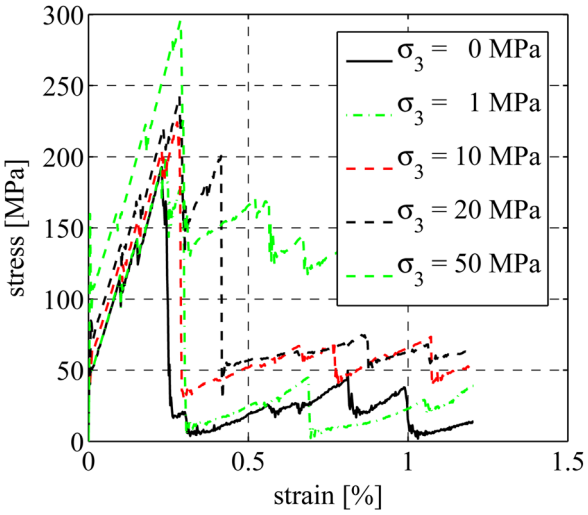

Fig. 1 Stress-strain curves for different confining pressures σ_3

Table 1 Comparison of friction angles Φ

Confinement σ_3	Granite [33]	Here	PFC3D [19]
1 MPa	61 deg	49 deg	–
10 MPa	58 deg	31 deg	32 deg

Stress-strain curves of an unconfined and a series of confined compression test simulations are depicted in Fig. 1. The curves do not start at zero stress for zero strain, i.e., $\sigma(\varepsilon = 0) \neq 0$, as the specimen is generated in a nonequilibrium state with unbalanced internal stresses. Upon presence of internal stresses the failure behavior of the model is slightly more realistic as compared to a model that is created in an equilibrium state.

The unconfined compressive strength of $C_0 \approx 200$ MPa and Young's modulus of $E \approx 65$ GPa are in agreement with typical values reported for granite [33]. A nearly complete brittle fracture is observed after a short interrupt of the failure process just after initiation of macroscopic failure. This indicates that the model exhibits so-called class II behavior as usually observed for granite [33,34]. The recovery of stress up to $\sigma \approx 50$ MPa after macroscopic fracture in uniaxial compression is due to the facts that a small portion of the cross section remains intact and that the crack surfaces of the two fragments are pressed against each other for continued loading. The latter is even more important for confined compression where it is related to the strength of the broken rock mass [32,35].

The increase of strength with confining pressure can be expressed in terms of Mohr-Coulomb friction angles [36]. In Table 1 the friction angles for low to medium confining pressures are compared to experimental values [33] and results from published 3D DEM simulations [19]. While for $\sigma_3 = 1$ MPa the friction angle is rather close to the experimental one, it is significantly lower for $\sigma_3 = 10$ MPa. A similar value was found in other DEM simulations using bonded spheres [19]. Thus, it might be suspected that a friction angle $\Phi \approx 30$ deg is an inherent property of bonded spheres DEM as long as the stress state is not explicitly considered for bond strength as in Refs. [37,38]. Despite these deficiencies, the model is considered to be useful for investigation of ballast strength as the loading conditions that cause failure of individual stones are not too far from uniaxial compression; see also Sec. 4.

3 Generation of Breakable Angular Ballast Stones

It is well known that the strength of an aggregate, e.g., of ballast stones, depends strongly on the shape and especially angularity of

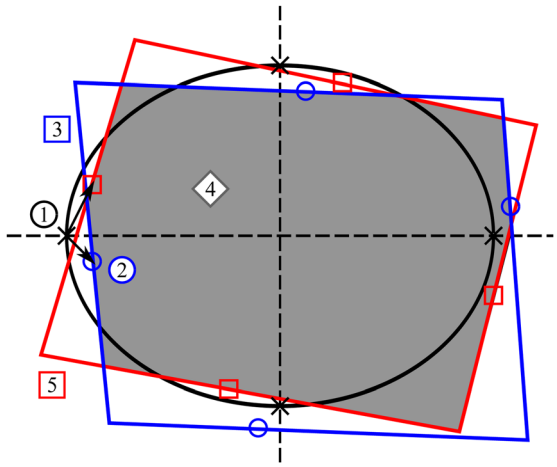

Fig. 2 Two-dimensional sketch of the ballast stone shaping approach

Fig. 3 A typical ballast stone

these ballast stones [39–43]. Furthermore, breakage of ballast stones plays an important role in degradation of ballasted beds. Thus, for numerical simulation a model is required that captures the shape as well as the strength of single ballast stones. A method is proposed here to generate angular ballast stones made from the breakable granular solid that is described in Sec. 2.

Single ballast stones are extracted from a large sphere packing by removal of the unnecessary particles. A method to find a mathematical description of the ballast stones is proposed, which is based on tangent planes on ellipsoids. A two-dimensional sketch of this procedure is depicted in Fig. 2. The starting point for generation of the tangent planes is the intersection points of the ellipsoid with its axes (1). In order to account for the irregular shape of real stones these intersection points are moved randomly on the surface of the ellipsoid and in normal direction (2). Finally, tangent planes are constructed in the shifted points (3) and the stone is defined as the volume that is enclosed by all of these planes (4). It is found that the double application of the procedure with six planes on the same ellipsoid results in realistic shape and angularity (5). However, the use of even more tangent planes at one time would result in more rounded stones as the base points are then more uniformly distributed.

This approach is motivated from the finding that ballast stones usually feature quite planar faces; see Fig. 3. Comparison of the sketch and the photo indicates that the described procedure is likely to generate realistically shaped ballast stones. Here, it is assumed that cutting through an irregular arrangement of spheres will produce a surface whose roughness is comparable to real ballast stones. It was noted in Ref. [42] that, with regard to aggregate strength, shape is much more important than roughness and friction. Yet, for further studies, it might be desirable to account explicitly for surface roughness and corrugation as in Ref. [12], where unbreakable clumps of overlapping spheres were constructed based on image analysis of real stones. Likewise, the shape of the stones could be refined using, e.g., image processing techniques. Two typical realizations of stones generated with the described approach are depicted in Fig. 4. It is apparent that planar faces and sharp edges are formed. The sharpness of the edges is blurred to a small extend by model resolution, i.e., particle size. The projection of the DEM-stones is clearly polygonal and compares well to the general shape of real stones.

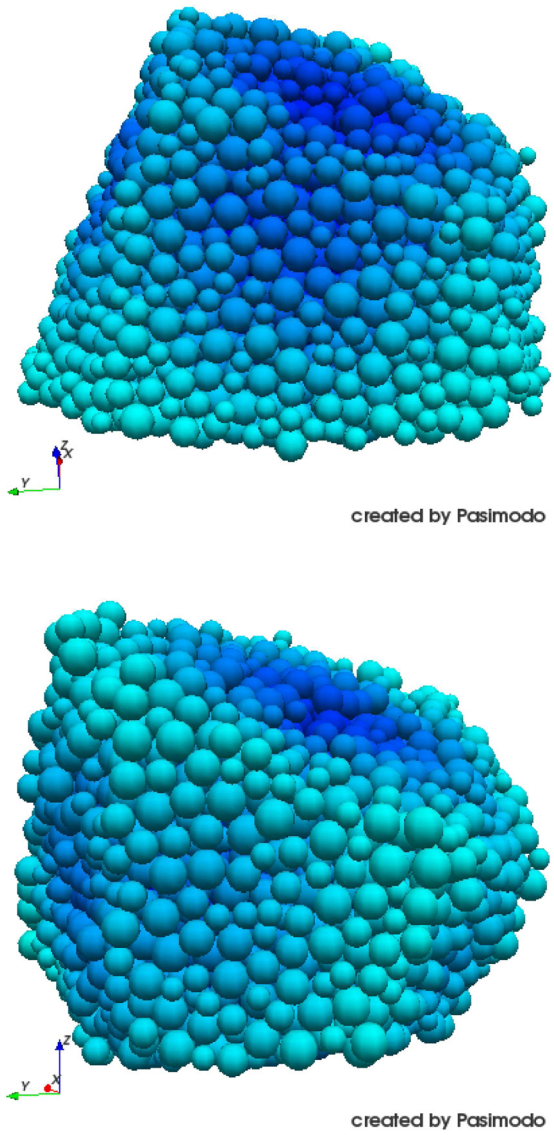

Fig. 4 Two realizations of ballast stones. Distance from the origin (located approximately at the center of the stones) color coded in order to clarify the shape.

The described procedure allows for simultaneous investigation of aspects that are mostly considered separately in current research papers. Breakable bonded particle DEM is conventionally applied to problems involving one breakable body of material such as excavations in rock; see, e.g., Ref. [19]. Applications to media composed of several breakable agglomerates are typically limited to geometrically simple shapes like disks or spheres [8,9]. Different approaches to create complex shaped agglomerates have been proposed [11,12], but they are limited to unbreakable materials as the particle arrangement is chosen according to the

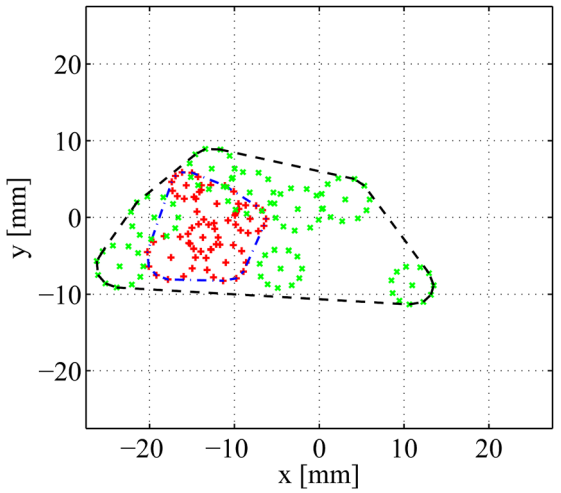

Fig. 5 Upper (dashed-dotted) and lower (dash) contact areas in a single stone compression test

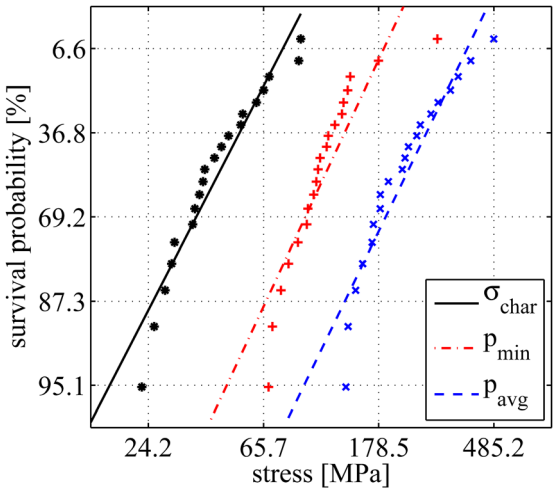

Fig. 6 Weibull plots of different measures of strength for $N = 700$

agglomerate geometry and not with respect to material behavior. The approach presented here unites elements of all mentioned areas on a mesoscopic level of detail. Yet, it allows studying the influence of particle breakage in ballast settlement and degradation with increased profundity.

4 Statistical Evaluation of Single Stone Strength

The strength of single ballast stones whose shape is obtained from the described approach and that consist of granular solid that resembles granite is investigated by compression between parallel platens [26]. This serves to verify that the model is able to predict the crushing strength of ballast stones. An extensive experimental study of the strength of single ballast stones is presented in Ref. [44]. There, the strengths of six types of ballast for various size fractions were investigated and quantified using Weibull statistics. For a given ballast and a given size fraction, the strengths are reported to follow the Weibull distribution [45] reasonably well. A characteristic strength is defined as the ratio of applied force F and the diameter d of the particle [44], i.e., platen distance at failure, as

$$\sigma_{\text{char}} = F/d^2. \tag{4}$$

For spherical bodies loaded with small contact areas this is a measure of the tensile stress acting in the central portion of the particle and it is obtained from elasticity theory [46]. An average strength σ_0 is defined as the value of the characteristic stress such that $1/e = 1/2.718... \approx 37\ \%$ of the particles survive [44].

In simulations, the contact areas of stone and platens can be extracted, which is not possible in experiments. Therefore, the smallest convex polygon enclosing a point-discretization of the perimeters of all contact particles is calculated yielding an estimate of the contact area. Figure 5 shows a typical plot of lower and upper contact areas. Due to the procedure similar to experiments of placing the stone between the platens, the lower contact area is usually larger than the upper one. The polygonal area is found to be approximately twice the cross-sectional area of all particles in contact with the loading platens. The polygonal area is considered to be the relevant quantity since the stress is distributed to adjacent particles and spacing between contact particles is usually less than two particle diameters. This means that it is assumed that a more homogeneous loading state over an area corresponding to the polygon is obtained slightly below the surface of the stone and that the loading conditions in this region are relevant for bulk fracture.

Table 2 Statistics of strength. Units of σ_0 and $p_{\text{min/avg},0}$ are MPa.

N	σ_0	m_σ	R^2_σ	$p_{\text{min},0}$	$m_{p,\text{min}}$	$R^2_{p,\text{min}}$	$p_{\text{avg},0}$	$m_{p,\text{avg}}$	$R^2_{p,\text{avg}}$
300	81.45	2.43	0.97	156.83	2.32	0.93	279.14	2.85	0.97
500	70.38	2.20	0.92	181.30	2.59	0.90	251.24	3.41	0.98
700	53.36	2.66	0.93	132.71	2.93	0.81	270.16	2.82	0.90
1000	49.65	2.30	0.97	134.80	2.27	0.95	289.56	2.93	0.91

Four sets of 20 stones comprising different numbers of particles were tested and subjected to a statistical analysis as described in Ref. [44]. The strength σ_{char} is calculated according to Eq. (4) and the contact pressures $p_{\text{min}} = F/A_{\text{max}}$ and $p_{\text{avg}} = 2F/(A_{\text{min}} + A_{\text{max}})$ are determined using the larger and the average contact area, respectively. Thereby, A_{max} and A_{min} denote the larger and smaller contact area between stone and platens, respectively. The average contact area is the mean value of the large and small contact area of one stone. The corresponding values are sorted in ascending order in a list, and for each failure stress a survival probability is calculated according to

$$P_s = 1 - k/(M+1) \tag{5}$$

where k is the rank of the stone in the list and M the total number of samples. If Weibull statistics apply, a plot of $\ln(\ln(1/P_s))$ against the logarithm of stress yields a straight line whose slope determines the Weibull modulus m, i.e. variability of strength.

The data points of a series of tests on 20 stones with about $N = 700$ particles and the lines of best fit are plotted in Fig. 6. The results indicate that the behavior of the DEM stones is not exactly Weibullian but reasonably close. Especially at lower strengths the data deviates a bit from the Weibull best fit. The shape of the plots of all measures of strength is comparable. Generally, a slight curvature to the right of especially σ_{char} and p_{avg}, but also p_{min}, is observed. This is in excellent agreement with the experimental results presented in Ref. [44]. The deviation for lower stresses is interpreted as a minimum strength, below which the probability of failure is zero.

The average strengths σ_0, $p_{\text{min},0}$ and $p_{\text{avg},0}$; the corresponding Weibull moduli m; and coefficients of correlation R^2 for tests on stones comprising different numbers N of particles are given in Table 2. The poor correlation of p_{min} for $N = 700$ is caused by one extremely strong stone in this particular measurement. Disregarding this stone, $R^2_{p,\text{min}} = 0.94$ is obtained.

The characteristic strength σ_0 clearly decreases with increasing particle numbers N. For $N = 700$ and $N = 1000$ values of about

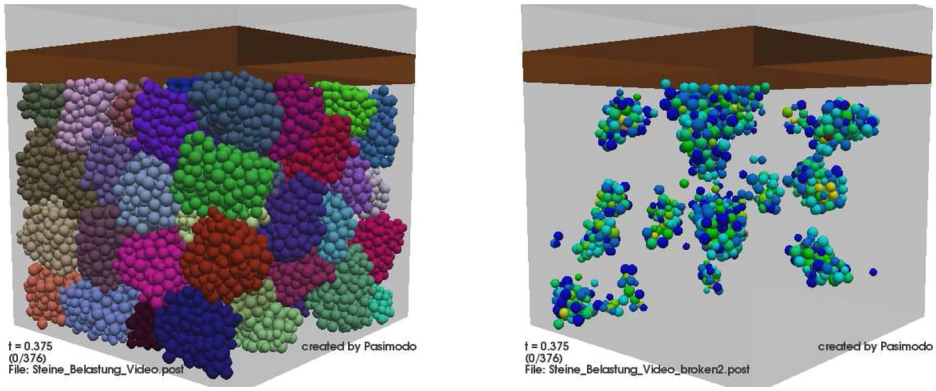

Fig. 7 Snapshot of an aggregate of 90 stones at the onset of catastrophic failure in oedometric compression. In the right picture only those particles are shown that have been involved in two or more bond breakage events.

$\sigma_0 \approx 50$ MPa are obtained, while the characteristic strength σ_0 is significantly higher for smaller particle numbers N. From uniaxial compression tests with varying cross section it is concluded that at least 700 particles per loaded volume element are required to assure discretization independent strength in the present model [27]. These numbers are confirmed by the single stone tests with respect to σ_0. As some of the particles do not contribute to the strength in diametral loading, the total number of particles per stone has to be somewhat higher. The minimum contact pressure $p_{\min,0}$ shows no clear trend, but a possible effect is weaker than for the characteristic strength σ_0, and it seems that convergence is reached at lower particle numbers. No dependence on particle numbers is detected for $p_{\text{avg},0}$, but the values fluctuate to some extent. Thus, the simulations indicate that the values of $p_{\min,0}$ and $p_{\text{avg},0}$ are less sensitive to particle numbers than σ_0.

The magnitude of σ_0 is higher here than reported in experiments on granite but comparable to small sized granodiorite ballast [44]. The simulations yield $\sigma_0 = 50$ MPa. In Ref. [44] experimental results are reported for granite and granodiorite, which is similar to granite in mineralogical composition and usually assumed to be slightly weaker than granite in terms of compressive strength. Thereby, $\sigma_0 = 12 - 33$ MPa and $\sigma_0 = 24 - 55$ MPa is obtained for large and small ballast stones, respectively. This means that the simulations show a tendency to overestimate the strength as compared to full size ballast. This might be due to two reasons. Firstly, the material model used here is calibrated to a compressive strength of $C_0 = 200$ MPa. But in DEM tensile strength is usually overestimated [15], which is important if the single particle crushing test evaluates tensile strength. In this model Brazilian tensile strength is approximately 20 MPa, whereas for granite tensile strength is about 10 MPa. Furthermore, in Ref. [44] no values of compressive strength are reported, so that it is not clear if the rocks tested there are as strong as assumed here. If tensile failure would be identified as the true mode of fracture, calibration could be made with respect to tensile strength.

The average contact area is about 600 mm^2 for stones comprising at least 500 particles, which would correspond to a contact radius of approximately 14 mm for a circular contact area. As the diameter of the stones is about 50 mm, the contact area is at the limit of being considered small according to Refs. [44,46]. Thus, fracture caused by tensile stresses might not be the determining mode of failure in these simulations.

The values of minimal and average contact pressure are found to be somewhat lower and higher than uniaxial compressive strength $C_0 = 200$ MPa, respectively. The finding that $p_{\text{avg},0} > C_0$ is reasonable, since this pressure acts near the loaded surface, and will have diminished slightly below the surface or in the center, where failure usually initiates. Hence, it might be suspected, that compressive strength and failure play a role in single particle crushing. As shown in Refs. [47,48], compressive failure in brittle rocks (and the DEM model, see Ref. [27]) is initiated by extensile cleavage parallel to the direction of maximum compression, which makes distinction between compressive and tensile failure awkward. Furthermore, it is pointed out in Ref. [49] that point load tests on spheres, which are similar to the ballast stone tests to some extent, provide a much more reliable estimate of the compressive strength than the tensile strength. This supports the notion that the contact pressures are related to the compressive strength and are of comparable magnitude.

The ratio of bonds failing in compression might serve as an indicator of the loading state, since compressive bond failure was identified as a means of fracture propagation, which is sensitive to loading conditions [27]. The percentage of compressive bond failure is about 30% for the single particle crushing tests, while it is 40% in uniaxial compression and 20% in uniaxial tension, respectively. Thus, it is concluded that failure of the stones does not occur in purely tensile conditions but that compressive stresses and strength are also important.

The average breakage strain, i.e., the relative difference of platen distance at the beginning and at failure, of stones consisting of at least 500 particles is approximately 4%. For the granite ballast investigated in Ref. [44] relative differences of 3.0%, 3.4%, and 5.6% are found for large, medium sized, and small ballast, respectively. Slightly higher values are reported for different granodiorite ballasts. The influence of contact stiffness in simulations and grinding of contact surface asperities in experiments on these values is not readily accessible. But from analysis of the simulation results it is estimated that, at least in simulations, the corresponding uncertainty is not exceeding 0.5%. Thus, the values of breakage strain obtained in simulations compare very well to the mentioned experiments. This gives further evidence of the sound calibration of the model and validates the simulative setup for single particle tests.

5 Failure of Ballast Aggregates

Aggregates of stones consisting of granular solid are constructed and loaded in order to verify the applicability of the presented simulation approach to assess degradation processes in ballast beds. Note, that in the presented model the ballast stones may break if their strength is exceeded. The shape of the stones changes due to the broken off fragments, which stay inside the simulation, i.e., fouling due to breakage and abrasion is captured by the simulation model.

5.1 Oedometric Compression of a Small Aggregate. As a first example, the oedometric compression of a small aggregate of stones is considered. In oedometric compression the aggregate is vertically loaded while lateral deformation is prohibited by rigid walls; see Fig. 7 left.

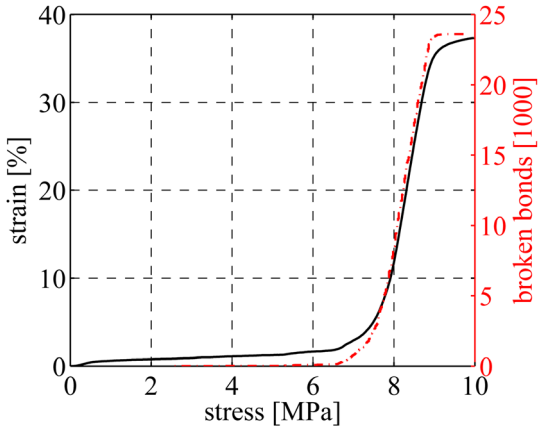

Fig. 8 Development of strain and breaking of bonds during stress controlled oedometric compression

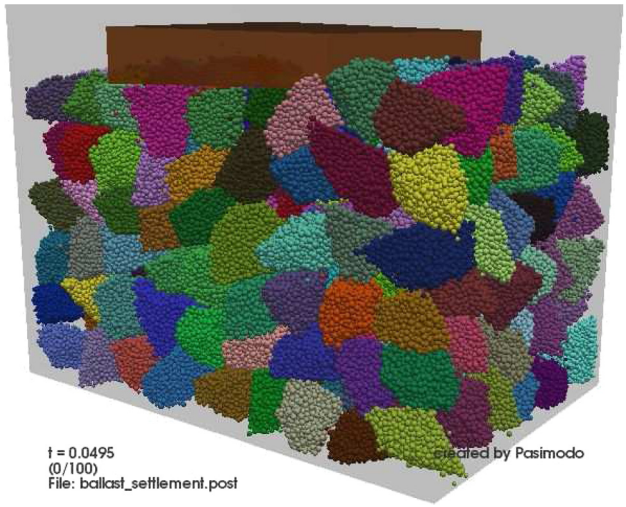

Fig. 9 Simulation of a ballast bed loaded by a sleeper

The aggregate is constructed by gravitational sedimentation and subsequent compaction at a constant vertical stress of 0.25 MPa. During the sedimentation process damping of the absolute motion of the particles is applied in order to speed up equilibration by increased dissipation at low frequencies [50,51]. The aggregate comprises 90 stones, each consisting of approximately 175 particles so that the total number of particles is about 15,800. The particle numbers are chosen to achieve reasonable computation times for first fundamental investigations of the model. Material parameters on bond level are adjusted to account for the particle number dependence of stiffness and strength that exists for breakable agglomerates with low particle numbers; see also Sec. 4 and Ref. [27].

The stiffness between spheres and walls is chosen as twice the stiffness between bonded spheres that do not belong to the same cluster in order to keep the overlap between spheres and walls small. Friction between particles and walls is not considered, as in experiments it is usually attempted to reduce wall friction due to its effect of making the strength measurement less reliable [52]. Also, friction between the stones is present only due to the roughness of their surfaces; an explicit friction coefficient is not introduced. For further research it is desirable to calibrate interstone friction based on experimental results. However, it is pointed out in Ref. [42] that the strength of an aggregate depends to a much larger extent on the shape of its constituents than on their roughness and friction. As for the present study the focus is on demonstrating the potential of the modeling approach, and the inherent roughness can be considered as sufficient to represent friction.

The aggregate is loaded with a continuously increasing vertical stress of up to 10 MPa. Vertical strain and the number of breaking particle bonds are recorded and plotted in Fig. 8. A further compaction of the aggregate is observed until the stress reaches 0.5 MPa. Then, up to a stress of 5 MPa strain increases linearly with stress and only an insignificant number of particle bonds is broken. Deformation of the specimen seems to be mostly resilient in this range. More frequent bond breakage events lead to a higher deformation rate between 5 and 6.5 MPa. At about 7 MPa the aggregate starts to collapse in a catastrophic manner until at 9 MPa the stones are almost completely crushed and no further breakage occurs. The final deformation is based on compaction of the broken fragments.

Figure 7 shows two pictures of the aggregate at a state when the specimen has just begun to collapse ($\sigma = 7.5$ MPa, $\varepsilon = 5.1\%$). On the left-hand side of Fig. 7 all particles are depicted, while on the right-hand side only those particles are shown, which have lost at least two bonds. It is found that most of the stones have not suffered any breakage, while some stones show minor damage and a few stones have been completely destroyed.

A complete breakdown of the aggregate is not observed in experimental tests. Here, it is attributed to the low resolution of the stones, which implicates a somewhat rude representation of failure processes. Furthermore, the stress controlled loading procedure boosts the collapse, whereas with strain controlled loading no breakdown would be observed. The simulation provides a yield stress of 7 MPa. This is somewhat higher than in experiments, where about 3 MPa are found [8,53]. However, the order of magnitude is caught approximately. Yet, the resolution of 4.5 stones per side of the cubic oedometer cell is too small to give resolution independent results. Thus, it cannot be expected to obtain equal stress values from simulation and experiments at higher size ratios and the fair agreement of simulative and experimental results is reasonable.

This demonstrates that the presented simulation approach is generally capable of describing the deterioration of ballast beds. An adequate resolution on both particle-stone and stone-aggregate level has to be assured in order to obtain quantitatively reliable results and to gain further insight into the failure process.

5.2 Indentation of a Sleeper in a Ballast Bed. Now the indentation of a sleeper in a ballast bed is investigated with a simplified model, which is based on the oedometer test. The box containing the ballast has a size of $0.495 \times 0.33 \times 0.33$ m and is loaded by a sleeper of length 0.2 m that covers the entire width; see Fig. 9. The top surface of the ballast beside the sleeper is uncovered to allow for rearrangement processes as in a ballasted railway track.

The aggregate consists of 324 stones each comprising slightly more than 1000 particles in average, resulting in a total of 331,000 particles. Stiffness and strength of the stones are shown in Sec. 4 and Ref. [27] to be widely independent of the particle number at a resolution of 1000 particles per stone.

The single stones are generated as described in Secs. 2 and 3. The collection of stones is then generated by an inflation procedure, which expands the single stones out of a dilute, non-overlapping cubic arrangement until the pressure on the surrounding walls starts to raise, i.e., when the aggregate is dense. The coordination number based growth rate approach as described in Sec. 2.1 is not applied here, instead all stones are expanded at the same rate. To save computation time, every stone is treated as one rigid body during specimen generation. The particles it consists of are only used for contact detection and calculation of contact forces. The equations of motion are numerically integrated for substitute particles with inertia properties calculated from the particles forming the stone. As in the sedimentation procedure damping of the absolute motion is applied.

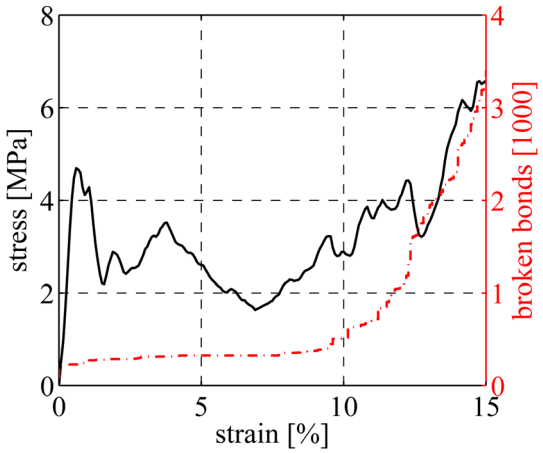

Fig. 10 Development of stress and breaking of bonds during strain controlled loading of a ballast bed

It was noticed, that the initial dilute arrangement of the stones has an impact on the structure of the resulting aggregate, although the stones are free to move in either direction upon first contacts during expansion. This means that the initial cubic arrangement will be reflected in the final specimen by the formation of columns of stones, which is unrealistic. Therefore, a random initial velocity of moderate magnitude is assigned to each stone so that the ordered arrangement is dissolved. The choice of the velocity magnitude is crucial as a too small velocity has no sufficient effect, whereas a high velocity is numerically problematic and will slow down the equilibration process. A maximal magnitude of $0.1\sqrt{3}$ m/s with uniform distribution and random direction of velocities was chosen here.

After these preparations the intended simulations can be started. For this simulation sphere to wall stiffness is chosen as 1/100 of bond stiffness in order to save computation time. With this lower stiffness overlap between particles and walls is still reasonably small. Regarding friction, the remarks from Sec. 5.1 apply here as well. The sleeper is slowly pressed into the ballast at a constant rate until a vertical strain of 15% is reached. The vertical strain is measured as the ratio of sleeper displacement to the initial height of the aggregate. Rotation of the sleeper is prevented. The development of the resultant stress (calculated using the area of the sleeper) and breakage of bonds are depicted in Fig. 10. As some preload results from the specimen generation procedure by expansion and as the contact stiffness is changed when the stones are converted to a granular solid, a small number of bonds is broken in the very first time steps. The effects of this breakage might be compared to the damage produced by vibration compaction in ballast installation.

Stress increases linearly with deformation until a maximum of 4.7 MPa is reached at 0.6% strain. Thereafter, the stress decreases and fluctuates between about 2 and 4 MPa while the number of broken bonds increases very slowly until the strain reaches 9%. This means that the deformation is based on densification and rearrangement of the stones. The stress level observed here is in agreement with the yield stresses in experimental oedometer tests [8,53].

Beyond 7% strain the stress shows a generally increasing trend towards 6.5 MPa at 15% strain. Starting at a strain of about 10% the deformation is no longer solely based on rearrangement, but the number of broken bonds increases strongly and the damaged stones allow for further compaction. Breakage is most prominent in the area below the sleeper where it is first noticed and then proceeds towards the bottom of the ballast box, as it might be expected. The bond breakage events are initially limited to the surface of the stones. Corners and faces in contact with corners are especially subject to damage. In an advanced stage of failure complete diametral breakage of a few stones is also observed. Again, this is consistent with experience. These processes are observed by detailed visual analysis of the system. However, due to the much higher particle numbers a simple picture like Fig. 7 (right) that visualizes the failure process gives no additional insight.

This second application example further illustrates, that the bonded particle approach is capable of describing all relevant stages of ballast bed deterioration starting from rearrangement over superficial damage to complete breakage of stones. Although the setup is not completely identical due to the open surface beside the sleeper, quantitative agreement of stress levels in the ballast bed simulation and experimental oedometer tests is observed. This gives evidence that the shape of the ballast stones and their arrangement in the aggregate are reasonable in the sense that the strength of the aggregate depends on these parameters as single particle strength was previously shown to comply with experimental results.

6 Summary and Conclusions

A discrete element model for the simulation of degradation processes in ballast beds has been presented. The model considers interaction and failure of individual ballast stones, which consist of breakably bonded particles.

The granular solid resembling strong rock, as, e.g., granite, is generated by bonding of adjacent particles of a dense packing. Highly dense sphere packings are obtained from a radius expansion procedure, which employs a particle's coordination number to control its growth rate. For bonding of particles a central force approach is applied that is enhanced by a progressive failure model in order to reproduce strength and failure modes of granite. The idea behind this model is to reduce the strength of bonds at particles that have been involved in previous bond breakage in order to facilitate instable crack propagation, which is no intrinsic feature of central force bonded granular solids. The model shows wide agreement of strength and failure properties as compared to granite.

An approach to generate angular ballast stones made from this granular solid is proposed. A number of tangent planes on ellipsoids of appropriate size and aspect ratios are used to define the volume of the stone. The strength of individual stones is assessed by diametral compression between parallel platens and compared to published experimental results. Very good qualitative and reasonable quantitative agreement is found by statistical evaluation. The stress state and the loading conditions that cause failure in this test setup are evaluated by analysis of different measures of strength and the importance of compressive strength is highlighted.

The applicability of this simulation approach to model ballast beds is demonstrated. Methods for generation of aggregates of stones are proposed and the importance of the numerical densification procedure is pointed out. Simulations of an oedometer test and the indentation of a sleeper in a ballast bed reveal that the model is able to describe rearrangement processes and superficial damage as well as complete breakage of stones. Thus, all stages of deterioration are covered by the model.

Research on ballast degradation might serve to develop a more profound understanding of the occurring phenomena, which helps to design methods to prevent track deterioration. This is of particular importance with increasing train speeds as they cause dramatically higher dynamic track loads that abet track failure [54]. The presented discrete element model is appropriate for this purpose, especially as simulations allow examination of quantities not observable in experiments. The procedures to generate ballast aggregates were identified as crucial and are worth further investigation. Simulations might also serve to assess the efficiency of reinforcement devices such as geogrids.

Acknowledgment

This work was partially funded by the German Research Foundation within the Collaborative Research Center SFB 716 "Dynamic Simulation of Systems With Large Numbers of Particles."

References

[1] Brown, S. F., Brodrick, B. V., Thom, N. H., and McDowell, G. R., 2007, "The Nottingham Railway Test Facility, UK," *Proceedings of the Institution of Civil Engineers/Transport*, **160**(TR2), pp. 59–65.
[2] Lackenby, J., Indraratna, B., McDowell, G. R., and Christie, D., 2007, "Effect of Confining Pressure on Ballast Degradation and Deformation Under Cyclic Triaxial Loading," Géotechnique, **57**(6), pp. 527–536.
[3] Tanabe, N., Matsumoto, N., Wakui, H., Sogabe, M., Okuda, H., and Tanabe, Y., 2008, "A Simple and Efficient Numerical Method for Dynamic Interaction Analysis of a High-Speed Train and Railway Structure During an Earthquake," J. Comput. Nonlin. Dyn., **3**(4), pp. 041002-1–8.
[4] Goicolea, J. M., Nguyen, K., Galbadón, F., and Bermejo, M., 2010, "Dynamic Analysis of High Speed Railway Traffic Loads on Ballast and Slab Tracks," Proceedings of the Tenth International Conference on Engineering Computational Technology, B. H. V. Topping, J. M. Adam, F. J. Pallarés, R. Bru, and M. L. Romero, eds., Valencia, Spain, 14–17 September 2010, Stirlingshire, U.K. Civil-Comp Press. Paper 18.
[5] Nishimura, K., Terumichi, Y., Morimura, T., and Sogabe, K., 2009, "Development of Vehicle Dynamics Simulation for Safety Analyses of Rail Vehicles on Excited Tracks," J. Comput. Nonlin. Dyn., **4**(1), pp. 011001-1–9.
[6] Zhai, W., and Wang, K., 2010, "Lateral Hunting Stability of Railway Vehicles Running on Elastic Track Structures," J. Comput. Nonlin. Dyn., **5**(4), pp. 041009-1–9.
[7] Cundall, P. A., and Strack, O. D. L., 1979, "A Discrete Numerical Model for Granular Assemblies," Géotechnique, **29**(1), pp. 47–65.
[8] Lim, W. L., and McDowell, G. R., 2005, "Discrete Element Modelling of Railway Ballast," Granul. Matter, **7**(1), pp. 19–29.
[9] Lobo–Guerrero, S., and Vallejo, L. E., 2006, "Discrete Element Method Analysis of Railtrack Ballast Degradation During Cyclic Loading," Granul. Matter, **8**(3-4), pp. 195–204.
[10] Lu, M., and McDowell, G. R., 2010, "Discrete Element Modelling of Railway Ballast Under Monotonic and Cyclic Triaxial Loading," Géotechnique, **60**(6), pp. 459–467.
[11] Lu, M., and McDowell, G. R., 2007, "The Importance of Modelling Ballast Particle Shape in the Discrete Element Method," Granul. Matter, **9**(1-2), pp. 69–80.
[12] Ferellec, J., and McDowell, G. R., 2010, "Modelling Realistic Shape and Particle Inertia in DEM," Géotechnique, **60**(3), pp. 227–232.
[13] Cho, N., Martin, C. D., and Sego, D. C., 2007, "A Clumped Particle Model for Rock," Int. J. Rock Mech. Min., **44**, pp. 997–1010.
[14] D'Addetta, G. A., Kun, F., and Ramm, E., 2002, "On the Application of a Discrete Model to the Fracture Process of Cohesive Granular Materials," Granul. Matter, **4**(2), pp. 77–90.
[15] Diederichs, M. S., 2000, "Instability of Hard Rockmasses: The Role of Tensile Damage and relaxation,". Ph.D. thesis, University of Waterloo, Canada.
[16] Fleissner, F., Gaugele, T., and Eberhard, P., 2007, "Applications of the Discrete Element Method in Mechanical Engineering," Multibody Sys. Dyn., **18**(1), pp. 81–94.
[17] Kun, F., and Herrmann, H. J., 1996, "A Study of Fragmentation Processes Using a Discrete Element Method," Comput. Meth. Appl. Mech. Eng., **138**, pp. 3–18.
[18] McDowell, G. R., and Harireche, O., 2002, "Discrete Element Modelling of Soil Particle Fracture," Géotechnique, **52**(2), pp. 131–135.
[19] Potyondy, D. O., and Cundall, P. A., 2004, "A Bonded-Particle Model for Rock," Int. J. Rock Mech. Min., **41**(8), pp. 1329–1364.
[20] Shimizu, H., Koyama, T., Ishida, T., Chijimatsu, M., Fujita, T., and Nakama, S., 2010, "Distinct Element Analysis for Class II Behavior of Rocks Under Uniaxial Compression," Int. J. Rock Mech. Min., **4**(2), pp. 323–333.
[21] Hentz, S., Daudeville, L., and Donzé, F., 2004, "Identification and Validation of a Discrete Element Model for Concrete," J. Eng. Mech., **130**(6), pp. 709–719.
[22] Wang, Y., and Tonon, F., 2011, "Dynamic Validation of a Discrete Element Code in Modeling Rock Fragmentation," Int. J. Rock Mech. Min., **48**(4), pp. 535–545.
[23] Cheng, Y. P., Nakata, Y., and Bolton, M. D., 2003, "Discrete Element Simulation of Crushable Soil," Géotechnique, **53**(7), pp. 633–641.
[24] Belytschko, T., and Black, T., 1999, "Elastic Crack Growth in Finite Elements With Minimal Remeshing," Int. J. Num. Meth. Eng., **45**(5), pp. 601–620.
[25] Bagi, K., 2005, "An Algorithm to Generate Random Dense Arrangements for Discrete Element Simulations of Granular Assemblies," Granul. Matter, **7**(1), pp. 31–43.
[26] Ergenzinger, C., Seifried, R., and Eberhard, P., 2010, "Failure of Geomaterials Assessed Using an Extended Discrete Element Method," Proceedings of the Seventh International Conference on Engineering Computational Technology, B. H. V. Topping, J. M. Adam, F. J. Pallarés, R. Bru, and M. L. Romero, eds., Valencia, Spain, 14–17 September 2010, Stirlingshire, U.K. Civil-Comp Press. Paper 136.
[27] Ergenzinger, C., Seifried, R., and Eberhard, P., 2011, "A Discrete Element Model to Describe Failure of Strong Rock in Uniaxial Compression," Granul. Matter, **13**(4), pp. 341–364.
[28] Gaugele, T., Fleissner, F., and Eberhard, P., 2008, "Simulation of Material Tests Using Meshfree Lagrangian Particle Methods," Proceedings of the Institution of Mechanical Engineers, Part K, [J. Multi-body Dynamics], **222**(4), pp. 327–338.
[29] Fleissner, F., 2010, "Parallel Object Oriented Simulation with Lagrangian Particle Methods," Dissertation, Schriften aus dem Institut für Technische und Numerische Mechanik der Universität Stuttgart, Band 16. Shaker Verlag, Aachen.
[30] Pasimodo, www.itm.uni-stuttgart.de/research/pasimodo/pasimodo_en.php.
[31] Ergenzinger, C., Seifried, R., and Eberhard, P., 2009, "Modelling of Crushable Ballast Using an Extended Discrete Element method," *Particle-Based Methods: Fundamentals and Applications*, E. Onate and D. R. J. Owen, eds., International Center for Numerical Methods in Engineering, pp. 134–137.
[32] Ergenzinger, C., Seifried, R., and Eberhard, P., 2012, "A Discrete Element Model Predicting the Strength of Ballast Stones," Comp. Struct.
[33] Martin, C. D., 1993, "The Strength of Massive Lac du Bonnet Granite Around Underground Openings," Ph.D. thesis, University of Manitoba, Winnipeg, Canada.
[34] Wawersik, W. R., and Brace, W. F., 1971, "Post-Failure Behavior of a Granite and Diabase," Rock Mech. Rock Eng., **3**(2), pp. 61–85.
[35] Hoek, E., and Brown, E. T., 1997, "Practical Estimates of Rock Mass Strength," Int. J. Rock Mech. Min., **34**(8), pp. 1165–186.
[36] Brady, B. H. G., and Brown, E. T., 2004, *Rock Mechanics for Underground Mining*, 3 ed., Kluwer Academic Publishers, Dordrecht.
[37] Wang, Y., and Tonon, F., 2009, "Modeling Lac du Bonnet Granite Using a Discrete Element Model," Int. J. Rock Mech. Min., **46**(7), pp. 1124–1135.
[38] Hentz, S., Donzé, F., and Daudeville, L., 2004, "Discrete Element Modelling of Concrete Submitted to Dynamic Loading at High Strain Rates," Comput. Struct., **82**(29-30), pp. 2509–2524.
[39] Lekarp, F., Isacsson, U., and Dawson, A., 2000, "State of the Art. I: Resilient Response of Unbound Aggregates," J. Transport. Eng., **126**(1), pp. 66–75.
[40] Lekarp, F., Isacsson, U., and Dawson, A., 2000, "State of the Art. II: Permanent Strain Response of Unbound Aggregates," J. Transport. Eng., **126**(1), pp. 76–83.
[41] Holtzendorff, K., 2003, "Untersuchung des Setzungsverhaltens von Bahnschotter und der Hohllagenentwicklung auf Schotterfahrbahnen," (in German), Dissertation, Technische Universität Berlin, Berlin.
[42] Cavarretta, I., Coop, M., and O'Sullivan, C., 2010, "The Influence of Particle Characteristics on the Behaviour of Coarse Grained Soils," Géotechnique, **60**(6), pp. 413–423.
[43] Stahl, M., and Konietzky, H., 2011, "Discrete Element Simulation of Ballast and Gravel Under Special Consideration of Grain-Shape, Grain-Size and Relative Density," Granul. Matter, **13**(4), pp. 417–428.
[44] Lim, W. L., McDowell, G. R., and Collop, A. C., 2004, "The Application of Weibull Statistics to the Strength of Railway Ballast," Granul. Matter, **6**(4), pp. 229–237.
[45] Weibull, W., 1951, "A Statistical Distribution Function of Wide Applicability," ASME J. Appl. Mech., **18**(3), pp. 293–297.
[46] Shipway, P. H., and Hutchings, I. M., 1993, "Fracture of Brittle Spheres Under Compression and Impact Loading. I. Elastic Stress Distributions," Philos. Mag. A, **67**(6), pp. 1389–1404.
[47] Fairhurst, C., and Cook, N. G. W., 1966, "The Phenomenon of Rock Splitting Parallel to the Direction of Maximum Compression in the Neighbourhood of a Surface," Proceedings of the First Congress of the International Society of Rock Mechanics, Lisbon, 25 September – 1 October 1966, vol. 1, pp. 687–692.
[48] Wawersik, W. R., and Fairhurst, C., 1970, "A Study of Brittle Rock Fracture in Laboratory Compression Experiments," Int. J. Rock. Mech. Min., **7**, pp. 561–575.
[49] Russell, A. R., and Muir Wood, D., 2009, "Point Load Tests and Strength Measurements for Brittle Spheres," Int. J. Rock Mech. Min., **46**(2), pp. 272–280.
[50] Jing, L., and Stephansson, O., 2007, *Fundamentals of Discrete Element Methods for Rock Engineering: Theory and Applications, Vol. 85 of Developments in Geotechnical Engineering*, Elsevier, Amsterdam.
[51] Luding, S., 2008, "Cohesive Frictional Powders: Contact Models for Tension," Granul. Matter, **10**(4), pp. 235–246.
[52] McDowell, G. R., Lim, W. L., Collop, A. C., Armitage, R., and Thom, N. H., 2004, "Comparison of Ballast Index Test for Railway Trackbeds," *Proceedings of the Institution of Civil Engineers/Geotechnical Engineering*, **157**(GE3), pp. 151–161.
[53] Lim, W. L., 2004. "Mechanics of Railway Ballast Behaviour," Ph.D, thesis, University of Nottingham, Nottingham, U.K.
[54] Yang, L. A., Powrie, W., and Priest, J. A., 2009, "Dynamic Stress Analysis of a Ballasted Railway Track Bed During Train Passage," J. Geotech. Geoenviron. Eng., **135**(5), pp. 680–689.